Experimental Insights on the NO-Dependent Yields of Aromatic Hydrocarbon Oxidation Products

AUTHOR NAMES.

Mengdi Song[1,4], Xin Li[1,3,*], Hendrik Fuchs[2,5], Anna Novelli[2], Philip T. M. Carlsson[2], Sören R. Zorn[2], Georgios I. Gkatzelis[2], Milan Roska[2], Ralf Tillmann[2], Franz Rohrer[2], Birger Bohn[2], Rongrong Wu[2,#], Sergej Wedel[2], Hui Wang[2], Shuyu He[1], Ying Liu[1], Andreas Wahner[2] and Yuanhang Zhang[1,3]

AUTHOR ADDRESS.

[1]State Key Laboratory of Regional Environment and Sustainability, College of Environmental Sciences and Engineering, Peking University, Beijing, 100871, P.R. China

[2]Institute of Climate and Energy Systems, ICE-3: Troposphere, Forschungszentrum Jülich GmbH, Jülich, 52428, Germany

[3]Collaborative Innovation Center of Atmospheric Environment and Equipment Technology, Nanjing University of Information Science & Technology, Nanjing, 210044, P.R. China

[4]School of Environment and Spatial Informatics, China University of Mining and Technology, Xuzhou, 221116, P.R. China

[5]Department of Physics, University of Cologne, Cologne, 50923, Germany

[#]J.C.S.: The University of Manchester, Manchester M13 9PL, United Kingdom.

***Correspondence to:** Xin Li (li_xin@pku.edu.cn)

Abstract Graphics

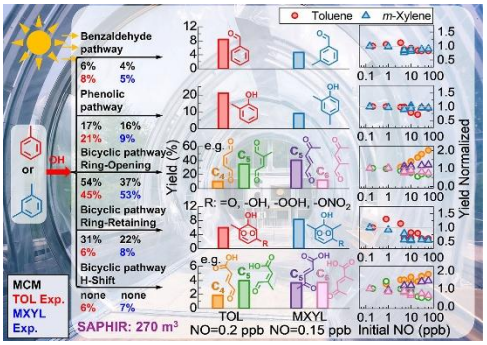

ABSTRACT

Aromatic hydrocarbons, play a critical role in the formation of urban ozone and secondary organic aerosols, impacting air pollution, climate change, and human health. However, their oxidation mechanisms remain uncertain, particularly under low nitric oxide (NO) conditions (<5 ppb). Using the SAPHIR chamber, this study investigated the yields of key oxidation products and their NO dependence under initial NO concentrations varying from 150 ppt to 20 ppb. For toluene (m-xylene) oxidation, the low-NO experimental yields of benzaldehyde, phenolic products, and products from bicyclic ring-opening, bicyclic ring-retaining, and H-shift reactions of organic peroxy radicals (RO_2) were 8% (5%), 21% (9%), 45% (53%), 6% (8%), and 6% (7%), respectively. The yields from the bicyclic pathway showed the strongest NO sensitivity. A comparison between the MCMv3.3.1 mechanism-simulated yields and experimental results revealed notable discrepancies, with model – measurement differences of +9% and +25% for the bicyclic ring-opening and ring-retaining products in toluene oxidation, and +7%, -16%, and +14% for the phenolic, bicyclic ring-opening, and ring-retaining products in m-xylene oxidation. Notably, products from H-shift RO_2 reactions, not included in the model, showed yields comparable to bicyclic closed-ring products, contributing 5–8% to carbon closure in toluene and 6–8% in m-xylene oxidation.

KEYWORDS. Aromatic hydrocarbons, Oxidation, Chamber experiments, Product Yields, NO-dependency, MCMv3.3.1

Synopsis

This study refines the experimental yields of benzaldehydes, phenolics, and products from bicyclic ring-opening, ring-retaining, and H-shift reactions of peroxide-bicyclic radicals in the photo-oxidation of aromatics under varying NO conditions.

INTRODUCTION

In the atmosphere, the oxidation of aromatics is mainly initiated by the reaction with hydroxyl (OH) radicals, and the subsequently formed oxidation products, most of which are semi-volatile or intermediate volatility organic compounds (S/IVOCs), play an important role in the formation of ozone (O_3) and secondary organic aerosol (SOA). The oxidation intermediates of aromatic hydrocarbons can be categorized into four classes[1] (Scheme 1): (1) Aldehyde pathway: aromatic aldehydes such as benzaldehyde and methylbenzaldehyde; (2) Phenol pathway: phenol, methylphenol, and polyhydroxylated aromatic phenols; (3) Bicyclic peroxide radical pathway: formaldehyde, glyoxal, methylglyoxal; and (4) Epoxide pathway: epoxides.

Although the oxidation of aromatics has been extensively studied over the past 20 years [2-6], large uncertainties remain in understanding the exact fate of short-lived radicals as well as the product distribution. For example, measured yields of cresol, glyoxal, and methyl glyoxal from the oxidation of toluene varies by factors between 5 – 18 in different studies[1, 4-8]. Moreover, previous experiments in the Simulation of Atmospheric Photochemistry In a Large Reaction Chamber (SAPHIR) showed a large discrepancy between measured and modeled oxidation intermediates or HOx (sum of OH and HO_2) radical concentrations [9, 10]. Only a few oxidation product yields have been measured due to the challenges in their quantitative detection, introducing considerable uncertainty into aromatic hydrocarbon oxidation research. In addition, a large part of the oxidation mechanisms is based on theoretical calculations, and there is a lack of comprehensive experimental insight into the distribution of aromatic hydrocarbon oxidation products under varying NO conditions. While our previous work focused on the oxidation of aromatic hydrocarbons under high-NO conditions (NO > 5 ppb, [NO]/[aromatic hydrocarbon] > 0.1) and revealed a significant NO-dependence in the product yields[11], the understanding of low-NO oxidation processes remains limited. In particular, data of experimental yields for reactions from some bicyclic retaining

reactions and recently found H-shift reactions under low-NO conditions is largely missing, representing a critical gap in the current knowledge. Therefore, laboratory studies on the oxidation processes of aromatic hydrocarbons under low-NO conditions can validate the applicability of the NO-dependencies of oxidation products and facilitate the refinement of aromatic hydrocarbon oxidation mechanisms.

With the advancements in measurement techniques and quantitative as well as semi-quantitative methods[12, 13], this study leverages the combined capabilities of mass spectrometry and spectroscopy to achieve comprehensive measurements of oxidation products. Using a large, atmospheric simulation chamber, the study focuses on the oxidation processes of aromatic hydrocarbons under initial NO mixing-ratios varying from 150 ppt to 20 ppb. The research identifies key intermediate species like benzaldehyde, phenolic products, and products from bicyclic peroxide reaction pathways during the oxidation of aromatic hydrocarbons. It further determines the branching ratios of major reaction pathways and the yields of critical intermediates under different initial NO concentrations scenarios, providing an evaluation of the accuracy of branching ratios in current models for aromatic oxidation pathways.

EXPERIMENTAL METHODS

The SAPHIR atmospheric simulation chamber.

The SAPHIR chamber is located at the Forschungszentrum Jülich in Germany. It has a cylindrical shape with a diameter of 5 m, a length of 18 m, and a total volume of 270 m^3. The chamber is made of a double layer of inert Teflon film and has a roof system that can be quickly opened and closed, allowing experiments to be conducted under both natural sunlight and dark conditions. To prevent contamination from the outside atmosphere, nitrogen gas (Linde, purity > 99.9999%) is continuously flushed between the double Teflon layers, maintaining an internal pressure approximately 45 Pa higher than the outside atmospheric pressure. The chamber is flushed with high-purity synthetic air, generated from liquid nitrogen (Linde, purity > 99.9999%) and liquid oxygen (Linde, purity > 99.9999%) to clean the chamber before each experiment. Humidification of the chamber air is achieved by evaporating Milli-Q water, which is then mixed with a high flow of synthetic air and flushed into the chamber. Gaseous reactants are introduced using calibrated mass flow controllers, while liquid reactants are injected via a micro syringe

through an injection port. The chamber is equipped with continuously running fans to ensure rapid mixing, with a mixing time of approximately 1 minute during the experiments. To compensate for sampling losses, high-purity synthetic air was added to the chamber. More detailed information regarding the SAPHIR chamber can be found in previous publications [9, 14].

In the SAPHIR chamber, the main source of radicals is the photolysis of HONO, leading to the production of OH radicals. The formation of HONO occurs photochemically at the chamber walls in the presence of water vapor [15]. The aromatic precursor and oxidation products generated by the reaction were measured by iodide-adduct time-of-flight chemical ionization mass spectrometry (I-CIMS), ammonium time-of-flight mass spectrometry (NH_4^+-VOCUS) and proton-transfer-reaction time-of-flight mass spectrometry (PTR-TOF-MS). A laser-induced fluorescence (LIF) instrument was used to measure OH radical concentrations. Chemiluminescence and UV absorption technology instruments were used to measure NOx and O_3, respectively. Photolysis frequencies were calculated from solar actinic flux measured by a spectroradiometer[16]. In this study, we focused on the gas-phase reactions and products of aromatics. Therefore, no particle-phase measurements were conducted. Detailed descriptions of the measurement instruments and their parameters are provided in Table S1.

Experimental Design.

The photochemical oxidation of toluene (initial concentration of 105 ppb) and m-xylene (initial concentration of 50 ppb) with OH radicals were investigated for different NO concentrations ranging from 150 ppt to 20 ppb and NO/aromatic concentration ratios from 0.002 to 0.2. The OH radical concentrations during the photochemical reaction ranged from 2.7×10^6 molecule cm^{-3} to 7.9×10^6 molecule cm^{-3}. All experiments were performed in synthetic air generated from high-purity N_2 and O_2, with O_2 maintained at atmospheric mixing ratio (20.94±0.02 % mol/mol). The O_2 concentration was held constant across all experiments. Details of the experimental conditions, including precursor concentrations, NO levels, NO/aromatic concentration ratios, and OH concentrations, are summarized in Table S2.

The experimental procedure is shown in Figure S1. Before the experiment, the chamber was cleaned with dry synthetic air, throughout the night. The chamber air was humidified to approximately 50% to 60% relative humidity. Then, the VOC precursor and NO were injected into the chamber, and the roof was opened 30 minutes later. After opening the roof of the chamber, nitrous acid (HONO) was photo-chemically formed on the chamber wall. The photolysis of HONO

led to the formation of OH radicals, which triggered the atmospheric oxidation reaction of aromatic hydrocarbons. The photochemical reactions were allowed to proceed for 5–6 hours before the chamber roof was closed.

Quantification of Aromatic Oxidation Product Yields.

During the experiments, the bicyclic ring-retaining products (such as bicyclic carbonyls, bicyclic alcohols, bicyclic hydroperoxides, and bicyclic nitrates) as well as more highly oxidized products formed during the oxidation of aromatic compounds were quantified by an I-CIMS instrument (TOFWERK) with a mass resolution (m/Δm) of 2500 to 3000. The dicarbonyls products (dimethyl-butenedial, and dimethyl-furanone) were quantified by an NH_4^+-VOCUS instrument (TOFWERK) with a mass resolution (m/Δm) of 8000–10000. The precursors (toluene and m-xylene), aldehydes (benzaldehyde, and tolualdehyde), phenols (cresol and xylenol), and dicarbonyls (methylglyoxal, butenedial, methylbutenedial and furanone, etc.) were measured by a PTR-TOF-MS instrument (PTR8000, Ionicon GmbH) with a mass resolution (m/Δm) of 3000 to 4000. In the I-CIMS instrument, neutral molecules (X) react with iodine ions (I^-) to produce product ions (XI^-) [17]. NH_4^+-VOCUS instrument uses ammonium–water cluster ($NH_4^+ \cdot H_2O$) as the reagent ion, and neutral molecules (X) react with $NH_4^+ \cdot H_2O$ to form product ions ($X \cdot NH_4^+$)[18]. PTR-TOF-MS uses hydronium ions (H_3O^+) as an ion source, and the neutral molecule (X) undergoes a proton transfer reaction with H_3O^+ to form the product ions (XH+) [19]. The instruments were calibrated for the precursor species and oxidation products using standard gas cylinders and a liquid calibration unit using concentrations from tens of ppt to several ppb. Further details of the quantitative and semi-quantitative methods of I-CIMS, NH_4^+-VOCUS and PTR-TOF-MS are presented in Section S1, Section S2 and Section S3.

The product yield is the amount of product generated per unit of precursor consumed. The products generated by the reaction between the precursor and the OH radical (R1) can also participate in the subsequent reactions, which mainly include reactions with the OH radical and O_3 (R2), photolysis reactions (R3), wall loss (R4) and dilution (R5).

$$ARO + OH \xrightarrow{k_{OH}} Product_1 + Product_2 + Product_3 + \ldots \quad (R1)$$

$$Product_i + OH/O_3 \xrightarrow{k_{i,OH}/k_{i,O_3}} Subsequent\ Product \quad (R2)$$

$$Product_i + hv \xrightarrow{J_{Product_i}} Subsequent\ Product \quad (R3)$$

$\text{Product}_i \xrightarrow{k_{\text{wall loss}}} \ldots$ (R4)

$\text{Product}_i \xrightarrow{k_{\text{dilution}}} \ldots$ (R5)

These subsequent reactions need to be corrected for the time period when the yield of products is calculated, and the concentration of product X at time i after correction can be calculated iteratively using Eq. (1) and (2). [6, 20]

$$[X]_{\text{corr.i}} = [X]_{\text{corr.i}-1} + [X]_{\text{meas.i}} - [X]_{\text{meas.i}-1} + k_{X,\text{loss}}\,[OH]_{i-1}[X]_{\text{meas.i}-1}\Delta t \quad (1)$$

$$k_{X,\text{loss}} = k_{X,OH} + \frac{k_{X,O_3}[O_3]_{i-1}}{[OH]_{i-1}} + \frac{J_X + k_{X,\text{wall loss}} + k_{X,\text{dilution}}}{[OH]_{i-1}} \quad (2)$$

$[X]_{\text{corr}}$ represents the concentration of product X after correction. $[X]_{\text{meas}}$ represents the measured concentration of product X. Δt is the time interval between time points i and (i-1). OH concentrations ([OH]) in all experiments were measured by a LIF instrument. The rate coefficients of the OH and O_3 reactions (k_{OH} and k_{O3}) with precursors and products were taken from the Master Chemical Mechanism version 3.3.1 (MCMv3.3.1) (http://mcm.york.ac.uk). The photolysis frequencies of the products (J_X) were obtained from the measured photolysis rates using the spectroradiometer, such as J_{NO_2}, J_{GLY} and J_{MGLY}. Other unmeasured photolysis frequencies were estimated using the MCM v3.3.1 parameterization under clear sky conditions [21]. To account for the effects of cloud cover and Teflon film in the chamber, these estimates were corrected by multiplying them with the ratio of measured to modeled NO_2 photolysis frequencies[22]. The resulting adjusted photolysis rates, are presented in Table S3. The wall loss rate of the products ($k_{X,\text{ wall loss}}$) in the chamber was calculated by an empirical formula [23-26]. In this study, the wall loss rate ranged from 7.5×10^{-7} to 5.7×10^{-5} s^{-1},with an uncertainty of 15%-20%[11, 24], and the details are shown in Section S4. The dilution rate coefficient of the products ($k_{X,\text{ dilution}}$) in the chamber was estimated from flow controller readings. Product yields were determined from the slopes of the regression between the calibrated concentrations of the products formed and the amounts of precursor reacted. Linear fitting was performed using data points from the initial stage of the reaction (typically within the first hour), when precursor conversion is low and primary product formation dominates. This approach minimizes the influence of subsequent oxidation processes, wall loss, and gas-particle partitioning on the determination of primary product yields. The yield fitting plots of the major oxidation products of toluene and m-xylene obtained from the experiments are shown in Figure S6 and Figure S7. Among them, the reactions with OH radicals

and photolysis reactions have significant impacts on the product yield. The uncertainty in the yield calculations arises from various factors, including measurement uncertainty, reaction rate uncertainty (including k_{OH} and $k_{O3,}$ $J_{X,}$ and $k_{wall\ loss}$), and linear regression uncertainty. In previous studies, we reported that the uncertainty range for the yields of different oxidation products in aromatic hydrocarbon oxidation is between 19% and 39%, with the uncertainty for most products being approximately 30% [11]. The measurement uncertainty for the products listed in Table S1. The reaction rate coefficient uncertainty, as reported in previous studies[11], is approximately 23% and the uncertainty associated with the linear regression is approximately 4%. In total, using the error propagation formula, we estimate the total uncertainty in the yield of directly quantifiable products from the benzaldehyde and phenolic pathways to be 20%, the uncertainty in the yield estimation for species measured by the PTR-TOF-MS instrument was 30%, while that for species measured by the I-CIMS and NH_4^+-VOCUS instrument was around 40%.

Box Model Simulations.

The product yields of OH-initiated toluene and m-xylene oxidation depend on NO levels[27]. Here we use a box model coupled with MCMv3.3.1 mechanism to simulate the theoretical yields under different NO conditions. The model was constrained by measured parameters including temperature (298K), pressure (1006 hPa), humidity (55%), photolysis frequencies (JNO_2, 4.2×10^{-3} s^{-1}), and dilution rate coefficients (1.5×10^{-2} h^{-1}) in the SAPHIR chamber. Simulations were performed independently for toluene and m-xylene oxidations. The initial mixing ratio was set to 100 ppb for toluene and to 50 ppb for m-xylene. Whereas initial NO concentrations was set to values ranging from 5 ppt to 500 ppb during different model runs. Given that the OH radicals in the chamber experiments are primarily derived from the HONO generated by the chamber wall effect, the model was constrained to the measured concentration of HONO. The model was operated at time dependent mode with a time step of 1 minute. The yield calculations were further refined by incorporating adjustments for subsequent reactions with OH and O_3 radicals (R2), photolysis processes (R3), and dilution effects (R5). The model yield uncertainties were estimated to be 20%, mainly stemming from uncertainties of reaction rate constants in the MCMv3.3.1[28-36]. The yield fitting plots for the major oxidation products of toluene and m-xylene simulated by the model are shown in Figure S8 and Figure S9.

RESULTS AND DISCUSSION

Distribution of Aromatic Oxidation Products.

In this study, more than 500 molecules were identified using I-CIMS during the photo-oxidation process of toluene and m-xylene with OH radicals. The relationship between mass defect and the mass-to-charge ratio (m/z) is depicted in Figure 1 a-b. Mass defect refers to the deviation between the exact mass and nominal mass of a product. Iodides exhibit a significant negative mass defect, which becomes more pronounced as the O/C ratio increases. As shown by the blue arrows in Figure 1 a-b, for species with identical carbon and hydrogen atom counts, the number of oxygen atoms correlates with the degree of oxidation, where higher oxidation corresponds to a larger negative mass defect. Conversely, for each additional -CH_2 group (as indicated by the red arrows), the oxidation degree decreases, resulting in a smaller negative mass defect. Regarding the evolution of the O/C ratio of product concentrations (Figure 1 c-d), products with low O/C ratios first increase and then decrease during the oxidation process. Small molecules with high O/C ratios, such as formaldehyde and glyoxal, increase in concentration throughout the reaction, becoming dominant components of the gaseous products.

The time series of products from specific reaction pathways and major products during toluene and m-xylene oxidation under different NO initial concentration ratios are shown in Figure S10 and S11. In terms of concentrations, bicyclic pathway products have the highest concentrations and are the dominant reaction pathway in the aromatic hydrocarbon oxidation process. The concentration of H-shift reaction products is comparable to that of benzaldehyde pathway products, and in the case of m-xylene oxidation, it even matches the concentration of phenolic pathway products, indicating a significant contribution to the overall oxidation process. During the 5-hour toluene oxidation, the concentrations of cresol, C_4 and C_5 unsaturated γ-dicarbonyls initially increase rapidly and then decrease slowly. As they undergo further oxidation with OH radicals or photolysis, their consumption rates are eventually higher than their production rates, resulting in a decline in concentration. The oxidation products of m-xylene follow the same trend. The NO concentration influences the peak concentration and peak time of phenolic and bicyclic pathway products but has a minimal effect on the peak concentration of benzaldehyde pathway products (Figure S10).

Benzaldehyde Pathway.

The photochemical oxidation mechanism of aromatic hydrocarbons with OH radicals is shown in Scheme 1. When aromatic hydrocarbons react with OH, the reaction branches into hydrogen abstraction and hydroxyl addition reactions [37, 38]. Among these, the hydrogen abstraction reaction is the main pathway for the formation of aromatic aldehydes, known as the benzaldehyde pathway (Scheme 1) [4, 39, 40]. The primary products for the benzaldehyde pathway during toluene and m-xylene oxidation are benzaldehyde (C_7H_6O) and methylbenzaldehyde (C_8H_8O), respectively. The yield of aromatic aldehyde compounds during the oxidation of toluene and m-xylene are shown in Figure 2 a and b. The yield of benzaldehyde from toluene oxidation, as reported in various studies, spans from 5% to 11% [5, 11, 41-46] (Table S5). The average yield of benzaldehyde obtained from toluene in this study was (8.2 ± 0.8)%. The yield of methylbenzaldehyde reported in different studies for m-xylene oxidation ranges from 3% to 9% [11, 41, 47-49] (Table S5). In this study, we experimentally determined that the yield of methylbenzaldehyde from m-xylene was (4.2 ± 0.5)%.

In this study, the NO initial concentration ratio is used to represent the influence of NO levels. A ±20% deviation from the calculated yield values of the MCMv3.3.1 mechanism is applied to assess the accuracy of the mechanism in simulating benzaldehyde pathway yields. From the variation of yields for toluene and m-xylene under different initial NO concentrations reported in the literature (Figure 2a and 2b), it can be observed that, under low NO conditions, the yield of methylbenzaldehyde decreases with increasing initial NO concentrations. On the one hand, higher NO concentrations promote the formation of the bicyclic nitrates; on the other hand, they shift the reaction towards the bicyclic ring-opening pathway. However, since the yield of benzaldehyde pathway is relatively low, this effect is rather small. Under high NO conditions, where the initial NO concentrations is greater than 10 ppb, the branching ratio of the benzaldehyde pathway shows no significant dependence on NO. Under low NO conditions, the benzaldehyde yield observed in this study slightly exceeds the predicted range of the MCMv3.3.1 mechanism, which is similar to the findings of Zaytsev et al. [46]. However, under high NO conditions, the yield is consistent with the predictions made by the MCM model calculations. The observed trend is generally consistent with most published data; however, some exceptions remain. For instance, in the studies by Ji et al. and Zhao et al., the yields of benzaldehyde and methylbenzaldehyde were (11.3 ± 2.0)% [5] and 6.4% – 8.7% [49], respectively, which are significantly higher than the values calculated using the

MCM. This discrepancy may be due to the influence of the O_2 concentration. Zhao et al. discussed the variation in the methylbenzaldehyde yield under different O_2 concentrations, showing that at lower O_2 concentrations, the yield of methylbenzaldehyde increases [49].

Phenolic Pathway.

The aromatic–OH adducts formed during the addition reaction between aromatic hydrocarbons and OH radicals can further react with O_2, branching into hydrogen abstraction and O_2 addition pathways. When aromatic–OH adducts undergo hydrogen abstraction reactions by O_2, this becomes the main pathway for the formation of phenolic products [4, 5, 39], known as the phenolic pathway (Scheme 1). The primary products for the phenol pathway during toluene and m-xylene oxidation are cresol (C_7H_8O) and xylenol ($C_8H_{10}O$), respectively. The laboratory yields and MCMv3.3.1 simulated yields of cresol and xylenol from the toluene and m-xylene oxidation under different initial NO concentrations are shown in Figure 2c and d. The yields for the cresol and xylenol oxidation in various studies are reported as 10% to 53% [5, 11, 43-46, 50] and 8.2% to 25%[11, 47-49], respectively (Table S5).

The average yield of cresol obtained in this study was (18.9 ± 2.5)%, which is consistent with the 14.5–21% range reported by Klotz et al. [44] and the 17.9% reported by Smith et al. [45]. This yield is also consistent with the value of 18% for cresol predicted from calculations using the MCMv3.3.1 mechanism. The yield of xylenol obtained in this study was (8.8 ± 0.5)%, which is in good agreement with our previous report under high NO conditions (8.2%–8.6%) [11] and the 11% reported by Smith et al. [48]. In contrast, the MCMv3.3.1 mechanism predicts a yield of approximately 17%, which is much higher than both the experimental results from this study and previous reports. This suggests the need for modifications of the mechanism regarding the phenolic pathway of m-xylene. The yield of the phenolic pathway shows no significant dependence on the NO concentration (Figure 2c and d). Moreover, as with the aldehyde pathway, the phenolic pathway yield is also influenced by the O_2 concentration. This explains why Ji et al. [5] and Zhao et al. [49] reported significantly higher yields for the phenol pathway compared to other studies.

Bicyclic Pathway: Ring-Opening Products.

Aromatic–OH adducts can undergo addition reactions with O_2 to form bicyclic peroxy radicals, a process referred to as the bicyclic pathway. Within this pathway, when bicyclic peroxy radicals

undergo ring-opening reactions, they can produce C_2−C_3 α-dicarbonyls and C_4−C_6 unsaturated γ-dicarbonyls (Scheme 1) [38, 51, 52]. The primary products for the ring-opening products in the bicyclic pathway during toluene and m-xylene oxidation include glyoxal ($C_2H_2O_2$), methylglyoxal ($C_3H_4O_2$), butenedial and its isomers ($C_4H_4O_2$), methylbutenedial and its isomers ($C_5H_6O_2$), and methyl-4-oxo-2-pentenal and its isomers ($C_6H_8O_2$) [4, 8, 53, 54]. The yields of C_2-C_6 ring-opening products from the aromatic peroxy-bicyclic pathway reported in various studies show significant variation and a strong NO dependence (Figure 3). For toluene oxidation, the yield range for glyoxal is 4% to 39% [8, 41, 43, 45, 46, 50, 51, 55-58], for methylglyoxal it is 4% to 37% [8, 11, 41, 43, 45, 46, 50, 51, 55, 56, 58], for $C_5H_6O_2$ it ranges from 6% to 37% [11, 45, 46, 58], and for $C_4H_4O_2$ it ranges from 8% to 24% [11, 46, 50, 58]. For m-xylene oxidation, the yield range for glyoxal is 8% to 13% [8, 41, 48, 51, 52], for methylglyoxal it ranges from 10% to 52% [8, 11, 41, 48, 49, 51, 52], for $C_6H_8O_2$ it ranges from 3% to 11% [11, 49], and for $C_5H_6O_2$ it ranges from 9% to 49% [11, 48, 49]. Detailed information on the yields of aromatic hydrocarbon oxidation products from previous literature and this study can be found in Table S5.

In this study, the yield of glyoxal from toluene oxidation ranged from 22% to 27%, and the yield of methylglyoxal ranged from 17% to 21%. Within the initial NO concentrations range of 0.2 to 20 ppb, the yields of glyoxal and methylglyoxal initially increase and then decrease as NO concentration rises, with a turning point observed at an initial NO concentrations around 3.5 ppb (Figure 3a and b). This pattern can be attributed to the fact that, under low NO conditions, the reaction predominantly favors the formation of open-ring products. However, at higher NO concentrations, the competitive effects of subsequent multi-generational reactions involving glyoxal and methylglyoxal lead to a reduction in their yields. The MCMv3.3.1 mechanism predicts glyoxal and methylglyoxal yields of 27%–44% and 20%–29%, respectively, which also show an initial increase followed by a decrease with increasing NO concentration, but these values are significantly overestimated compared to this study and previous experimental results (Figure 3a and b). In the oxidation of m-xylene, the yields of glyoxal and methylglyoxal are 12%–14% and 53%–58% (Figure 3e and f), respectively, which are higher than the predictions from the MCM model. Similar to toluene oxidation, the yield of methylglyoxal from m-xylene oxidation also shows an initial increase followed by a decrease with increasing NO concentration. The ratio of glyoxal to methylglyoxal in toluene and m-xylene oxidation is approximately 1.24 and 0.23, respectively, showing no significant dependence on NO concentration (Figure S12).

In the ring-opening reaction of bicyclic alkoxy radicals within the bicyclic pathway, unsaturated γ-dicarbonyls (C_4-C_6) are generated alongside glyoxal and methylglyoxal. In this study, within the initial NO concentrations range of 0.2 to 20 ppb, the experimental yields of $C_5H_6O_2$ and $C_4H_4O_2$ are 19–35% and 10–17% (Figure 3c and d), respectively. As NO concentration increases, the yield of $C_5H_6O_2$ shows a noticeable decreasing trend, while the yield of $C_4H_4O_2$ exhibits a significant increasing trend. This observation is consistent with the results obtained under high NO conditions in our previous experiments. The MCMv3.3.1 mechanism predicts yields of $C_5H_6O_2$ and $C_4H_4O_2$ in the ranges of 33–44% and 15–26%, respectively, with trends similar to those of glyoxal and methylglyoxal as NO concentration varies. This suggests that the MCM mechanism exhibits limitations in accurately simulating the formation and subsequent reactions of unsaturated γ-dicarbonyls (C_4-C_5), resulting in an overestimation of $C_5H_6O_2$ at high NO concentrations and an overestimation of $C_4H_4O_2$ at low NO concentrations. Similar to toluene, during the oxidation of m-xylene, the yield of $C_6H_8O_2$ decreases significantly with increasing NO concentration, while the yield of $C_5H_6O_2$ shows a clear increasing trend. Within the initial NO concentrations range of 0.15 to 10 ppb, the yields of $C_6H_8O_2$ and $C_5H_6O_2$ were found to be 9–12% and 41–46% (Figure 3g and h), respectively. The MCMv3.3.1 mechanism predicts yields of $C_6H_8O_2$ and $C_5H_6O_2$ to be 7–10% and 29–45%, respectively, showing an underestimation of the $C_5H_6O_2$ yield. Under low NO conditions, the $C_5H_6O_2$/ $C_4H_4O_2$ and $C_6H_8O_2$/ $C_5H_6O_2$ ratios for both toluene and m-xylene oxidation range from 1.15 to 3.38 and 0.21 to 0.30, respectively, both of which exhibit a significant decreasing trend as NO concentration increases (Figure S12).

Bicyclic Pathway: Ring-Retaining Products.

In the bicyclic pathway, bicyclic peroxy radicals can react with NO, RO_2, and HO_2 in bimolecular reactions, leading to the formation of bicyclic alkoxy radicals and various ring-retaining products, including bicyclic carbonyls, bicyclic alcohols, bicyclic hydroperoxides, and bicyclic nitrates (Scheme 1) [46, 59]. The primary products for the bicyclic pathway in toluene and m-xylene oxidation are bicyclic carbonyls ($C_7H_8O_4$ and $C_8H_{10}O_4$), bicyclic alcohols ($C_7H_{10}O_4$ and $C_8H_{12}O_4$), bicyclic hydroperoxides ($C_7H_{10}O_5$ and $C_8H_{12}O_5$), and bicyclic nitrates ($C_7H_9NO_6$ and $C_8H_{11}NO_6$). Previous studies have lacked laboratory reports on the yields of ring-retaining products such as bicyclic carbonyls, bicyclic alcohols, bicyclic hydroperoxides, and bicyclic nitrates during the oxidation of aromatics under low-NO conditions. In this study, within the initial

NO concentrations range of 0.2 to 20 ppb, the experimental yields of $C_7H_8O_4$, $C_7H_{10}O_4$, $C_7H_{10}O_5$, and $C_7H_9NO_6$ are 1.8–3.4%, 0.5–0.8%, 0.2–0.8%, and 1.7–3.2%, respectively (Figure 4a–d). Similarly, within the initial NO concentrations range of 0.15 to 10 ppb, the yields of $C_8H_{10}O_4$, $C_8H_{12}O_4$, $C_8H_{12}O_5$, and $C_8H_{11}NO_6$ are 1.4–3.8%, 0.6–1.8%, 0.1–0.6%, and 2.1–3.1%, respectively (Figure 4e–h).

A NO-dependence analysis reveals that the yields of bicyclic carbonyls and bicyclic alcohols formed during the oxidation of toluene and m-xylene exhibit a pronounced decline with increasing NO concentrations (Figure 4). This trend is similar to our previous findings and the predictions of the MCM mechanism. The primary reason for this behavior is the competition between RO_2 + NO reactions and RO_2 + HO_2/RO_2 reactions as NO concentrations increase [38]. Notably, under low-NO conditions, the yield of $C_7H_9NO_6$ initially increases and then decreases with rising NO concentrations, whereas the yield of $C_8H_{11}NO_6$ shows no significant dependence on the NO concentration. Compared to the MCM-predicted values for bicyclic ring-retaining products, our findings indicate that the MCMv3.3.1 mechanism significantly overestimates the yields of $C_7H_8O_4$, $C_7H_{10}O_5$, $C_7H_9NO_6$, $C_8H_{12}O_5$, and $C_8H_{11}NO_6$, while underestimating the yields of $C_7H_{10}O_4$ and $C_8H_{12}O_4$. However, it provides a reasonable simulation for the yield of $C_8H_{10}O_4$.

Bicyclic Pathway: Products from H-shift reactions.

In recent years, with the development of autoxidation theory, researchers have proposed two new hydrogen shift reactions for the aromatic hydrocarbon bicyclic pathway based on quantum chemical calculations. These are (1) a 1,5-aldehyde hydrogen shift [6, 60]and (2) a bicyclic peroxy radical hydrogen shift [40]. The important gas-phase H-shift products (Figure 5) in the bicyclic pathway during the toluene and m-xylene oxidation are 1,5-aldehyde H-shift products ($C_4H_4O_3$, $C_5H_6O_3$, and $C_6H_8O_3$) and bicyclic peroxy radical H-shift products ($C_7H_8O_6$ and $C_8H_{10}O_6$). Within the initial NO concentrations range of 0.2 to 20 ppb investigated in this study, the yields of $C_4H_4O_3$ and $C_5H_6O_3$ from the 1,5-aldehydic H-shift reaction[6, 60] were 1.9–2.8% and 2.2–5.6%, respectively (Figure 5a-b). For initial NO concentrations range of 0.15 to 10 ppb, the yields of $C_5H_6O_3$ and $C_6H_8O_3$ were 3.4–4.3% and 2.3–3.7%, respectively (Figure 5c-d). A NO-dependence analysis reveals that the yields of the two products from the bicyclic H-shift pathway exhibit opposing trends with increasing NO concentration. Similar to the bicyclic RO_2 ring-opening pathway, the H-shift ring-opening products are also generated through the reactions of alkoxy radical

intermediates with NO. This phenomenon may arise from competitive reaction pathways of isomeric alkoxy radical intermediates in relation to NOx[11]. Under low-NO conditions, the ratios of $C_5H_6O_3$ / $C_4H_4O_3$ and $C_6H_8O_3$ / $C_5H_6O_3$ during the oxidation of toluene and m-xylene were 0.85–2.35 and 0.58–1.01, respectively, both of which showed a significant decrease as NO concentration increased (Figure S12). Furthermore, the bicyclic peroxy radical H-shift products $C_7H_8O_6$ and $C_8H_{10}O_6$, formed via autoxidation reactions in the bicyclic pathway[40], were quantitatively measured, with yields remaining below 0.2%. These low concentrations indicate that their contribution to the gas-phase composition during the oxidation process is negligible. However, this may also be due to the fact that $C_7H_8O_6$ and $C_8H_{10}O_6$ belong to highly oxygenated organic molecules (HOMs), which have very low volatility and are prone to losses in particles[61]. Therefore, the overall contribution of the H-shift pathway (5–8%) is mainly derived from the 1,5-aldehyde H-shift products ($C_4H_4O_3$, $C_5H_6O_3$, and $C_6H_8O_3$).

ATMOSPHERIC IMPLICATIONS

This study leverages a large chamber simulation system to investigate the laboratory yields and NO-dependency of key products generated during the oxidation of aromatics under low-NO conditions. By summing the yields of key oxidation intermediates from each pathway, the branching ratios for individual reaction pathway were quantified (Figure 6). The branching ratios of different reaction pathways predicted by the MCMv3.3.1 mechanism under varying initial NO concentrations are presented in Figure S13. For initial NO concentrations range of 0.2 to 20 ppb, the branching ratios of the benzaldehyde pathway, phenolic pathway, and bicyclic pathway during toluene oxidation were determined to be 8%, 19%, and 54%, respectively (Figure 6a). For initial NO concentrations range of 0.15 to 10 ppb, the corresponding branching ratios for m-xylene oxidation were 4%, 9%, and 67%, respectively (Figure 6b). Including newly identified H-shift products (mainly from 1,5-aldehyde H-shift reactions) enhanced the experimental carbon flow by 6% for toluene and 7% for m-xylene. As a result, carbon closure increased from 75% to 81% for toluene and from 73% to 80% for m-xylene, reflecting the contribution of H-shift products to the overall carbon mass balance. The H-shift pathway exhibits a branching ratio comparable to that of the bicyclic ring-retaining pathway, which is known to significantly influence SOA formation[46]. In addition, H-shift reactions generate ROx and HOx radicals[40, 60] that can participate in the NO–NO_2–O_3 cycle and promote ozone formation[1], while the highly oxygenated organic products

(HOMs) can partition into particles and contribute to SOA formation[40]. This indicates that the H-shift pathway contributes substantially to the overall oxidation mechanism. Therefore, the H-shift pathway should not be overlooked in evaluating the atmospheric fate of aromatic compounds.

By combining the laboratory yields reported under high-NO conditions[11], it can be observed that the bicyclic pathway exhibits the strongest NO-dependence among all oxidation pathways (Figure 6). The branching ratio of the bicyclic pathway shows a trend of initially decreasing and then increasing with changes in the initial NO concentrations. Comparing the ratio of ring-opening products to ring-retaining products within the bicyclic pathway reveals an overall increasing trend with rising initial NO concentrations (Figure S12g-h). For unidentified oxidation products of toluene and m-xylene, their contributions account for 10–32% and 18–21% of the total carbon closure, respectively (represented as the "unknown" portion in Figure 6). Previous studies have suggested that these unidentified products primarily originate from the formation of highly oxygenated organic molecules (HOMs) formed via intramolecular H-shift reactions of bicyclic peroxy radicals, which are more prominent under low-NO conditions[40]. However, existing reports indicate that the yields of these HOMs from aromatic oxidation under low-NO conditions are less than 2% in the latest flow tube experiments [62]. Nonetheless, flow-tube experiments may underestimate HOM yields due to significant wall losses, and the NO-dependence of HOM yields is still unknown. This study finds that the proportion of unidentified products displays a trend of first increasing and then decreasing with changes in the initial NO concentrations. This behavior may arise from the complex factors influencing HOMs formation during aromatic oxidation[63-65], which do not follow a simple monotonic relationship with NO concentration. Theoretical calculations further indicate that additional HOMs can be produced from the subsequent oxidation of alkyl radicals generated via the 1,5-aldehyde hydrogen shift in the bicyclic pathway[6, 60], which may also serve as a potential source of the missing carbon. Therefore, the observed 10 – 32% unidentified fraction in the total carbon closure may result from a combination of HOMs formation, low-volatility gas-phase products, and under-detected particle-phase species. Further chamber experiments simultaneously measuring gas-phase and particle-phase products under different NO conditions are needed to identify the unknown components of aromatic oxidation.

Further comparison of the variation in model-to-experimental yield ratios for benzaldehyde, phenolic, and bicyclic pathways during toluene and m-xylene oxidation at different initial NO concentrations, as shown in Figure 6 and S14-15, reveals certain limitations in the MCM

mechanism's simulation of aromatic hydrocarbon oxidation. For example, it overestimates the branching ratio of the bicyclic ring-retaining pathway during toluene oxidation, as well as the branching ratios of the phenolic and bicyclic ring-retaining pathways during m-xylene oxidation, while underestimating the branching ratios of the bicyclic ring-opening pathway in m-xylene oxidation processes (Figure 6). From the perspective of product simulations, the MCM mechanism tends to overestimate the yields of glyoxal, methylglyoxal, $C_4H_4O_2$, $C_5H_6O_2$, $C_7H_8O_4$, and $C_7H_9NO_6$ in toluene oxidation, while underestimating the yield of $C_7H_{10}O_4$ (Figure S14). In m-xylene oxidation, MCM overestimates the yields of $C_8H_{10}O$ and $C_8H_{11}NO_6$, but underestimates the yields of glyoxal, methylglyoxal, $C_5H_6O_2$, and $C_6H_8O_2$ (Figure S15). These discrepancies may arise because the MCM mechanism (1) markedly overestimates the rate of the $RO_2 \rightarrow QOOH$ pathway (Figure 4) during the oxidation of toluene and m-xylene, overestimates the $RO_2 \rightarrow QONO_2$ pathway by approximately 2–4 times (Figures S14 – S15), and underestimates the $RO_2 \rightarrow QOH$ pathway by roughly 5–20 times (Figure S14-15); (2) overestimates the rate constants for hydrogen abstraction of aromatic–OH adducts by O_2 in the phenolic pathways of m-xylene oxidation by about a factor of 2 (Figure 6), while underestimating the addition of O_2 to aromatic–OH adducts to form RO_2 in the bicyclic pathways of m-xylene oxidation (Figure 6); and (3) lacks the representation of 1,5-aldehyde H-shift reactions of RO radicals[6, 60] and RO_2 H-shift reaction channels[40]. It is noteworthy that these estimated magnitudes are based on the assumption that the observed products mainly originate from the corresponding reaction channels and are inferred from model-to-experimental yield ratios. Overall, the branching ratios of key oxidation products and reaction pathways observed during toluene and m-xylene oxidation under different initial NO concentrations (particularly under low NO conditions) provide valuable experimental data for future mechanistic studies. Future work should apply more detailed mechanistic modeling to refine rate parameters and update the mechanism accordingly.

Associated Content

Supporting Information.

The Supporting Information is available free of charge at website.

Detailed description of product identification and quantification by I-CIMS, NH_4^+-VOCUS and PTR-TOF-MS; Wall loss correction methods; and chamber experiment parameters.

AUTHOR INFORMATION

Corresponding Author

Xin Li−State Key Laboratory of Regional Environment and Sustainability, College of Environmental Sciences and Engineering, Peking University, Beijing 100871, China; Collaborative Innovation Center of Atmospheric Environment and Equipment Technology, Nanjing University of Information Science & Technology, Nanjing, 210044, P.R. China; orcid.org/0000-0001-5129-4801; Email: li_xin@pku.edu.cn.

Authors

Mengdi Song−State Key Laboratory of Regional Environment and Sustainability, College of Environmental Sciences and Engineering, Peking University, Beijing 100871, China; School of Environment and Spatial Informatics, China University of Mining and Technology, Xuzhou 221116, P.R. China; orcid.org/0000-0002-9967-4499.

Hendrik Fuchs−Institute of Climate and Energy Systems, ICE-3: Troposphere, Forschungszentrum Jülich GmbH, Jülich 52428, Germany. Department of Physics, University of Cologne, Cologne 50923, Germany.

Anna Novelli−Institute of Climate and Energy Systems, ICE-3: Troposphere, Forschungszentrum Jülich GmbH, Jülich 52428, Germany.

Philip T. M. Carlsson−Institute of Climate and Energy Systems, ICE-3: Troposphere, Forschungszentrum Jülich GmbH, Jülich 52428, Germany.

Sören R. Zorn−Institute of Climate and Energy Systems, ICE-3: Troposphere, Forschungszentrum Jülich GmbH, Jülich 52428, Germany.

Georgios I. Gkatzelis−Institute of Climate and Energy Systems, ICE-3: Troposphere, Forschungszentrum Jülich GmbH, Jülich 52428, Germany.

Milan Roska−Institute of Climate and Energy Systems, ICE-3: Troposphere, Forschungszentrum Jülich GmbH, Jülich 52428, Germany.

Ralf Tillmann−Institute of Climate and Energy Systems, ICE-3: Troposphere, Forschungszentrum Jülich GmbH, Jülich 52428, Germany.

Franz Rohrer−Institute of Climate and Energy Systems, ICE-3: Troposphere, Forschungszentrum Jülich GmbH, Jülich 52428, Germany.

Birger Bohn−Institute of Climate and Energy Systems, ICE-3: Troposphere, Forschungszentrum Jülich GmbH, Jülich 52428, Germany.

Rongrong Wu−Institute of Climate and Energy Systems, ICE-3: Troposphere, Forschungszentrum Jülich GmbH, Jülich 52428, Germany; #aJ.C.S.:now at: The University of Manchester, Simon Building, Oxford Road, Manchester M13 9PL, United Kingdom.

Sergej Wedel−Institute of Climate and Energy Systems, ICE-3: Troposphere, Forschungszentrum Jülich GmbH, Jülich 52428, Germany.

Hui Wang−Institute of Climate and Energy Systems, ICE-3: Troposphere, Forschungszentrum Jülich GmbH, Jülich 52428, Germany.

Shuyu He−State Key Laboratory of Regional Environment and Sustainability, College of Environmental Sciences and Engineering, Peking University, Beijing 100871, China.

Ying Liu−State Key Laboratory of Regional Environment and Sustainability, College of Environmental Sciences and Engineering, Peking University, Beijing 100871, China.

Andreas Wahner−Institute of Climate and Energy Systems, ICE-3: Troposphere, Forschungszentrum Jülich GmbH, Jülich 52428, Germany.

Yuanhang Zhang−State Key Laboratory of Regional Environment and Sustainability, College of Environmental Sciences and Engineering, Peking University, Beijing 100871, China; Collaborative Innovation Center of Atmospheric Environment and Equipment Technology, Nanjing University of Information Science & Technology, Nanjing 210044, P.R. China.

Notes

The authors declare no competing financial interest.

ACKNOWLEDGMENT

This work was supported by the National Key R&D Program of China (grant no. 2022YFC3700201), the Beijing Municipal Natural Science Foundation (grant no. JQ21030), the

National Natural Science Foundation of China (grant nos. 91844301 and 91644108), and the EC-funded project ATMO-ACCESS Grant Agreement number 101008004.

REFERENCES

(1) Song, M.; Liu, Y.; Li, X.; Lu, S. Advances on Atmospheric Oxidation Mechanism of Typical Aromatic Hydrocarbons. *Acta Chim. Sinica.* **2021**, *79* (10), 1214-1231. DOI: https://doi.org/10.6023/a21050224.

(2) Bohn, B. Formation of Peroxy Radicals from OH−Toluene Adducts and O2. *J. Phys. Chem. A.* **2001**, *105* (25), 6092-6101 DOI: https://doi.org/10.1021/jp0033972.

(3) Suh, I.; Zhang, R.; Molina, L. T.; Molina, M. J. Oxidation mechanism of aromatic peroxy and bicyclic radicals from OH-toluene reactions. *J. Am. Chem. Soc.* **2003**, *125* (41), 12655-12665. DOI: https://doi.org/10.1021/ja0350280.

(4) Wu, R.; Pan, S.; Li, Y.; Wang, L. Atmospheric oxidation mechanism of toluene. *J. Phys. Chem. A.* **2014**, *118* (25), 4533-4547. DOI: https://doi.org/10.1021/jp500077f.

(5) Ji, Y.; Zhao, J.; Terazono, H.; Misawa, K.; Levitt, N. P.; Li, Y.; Lin, Y.; Peng, J.; Wang, Y.; Duan, L. Reassessing the atmospheric oxidation mechanism of toluene. *Proc. Natl. Acad. Sci. USA.* **2017**, *114* (31), 8169-8174. DOI: https://doi.org/10.1073/pnas.1705463114.

(6) Xu, L.; Moller, K. H.; Crounse, J. D.; Kjaergaard, H. G.; Wennberg, P. O. New Insights into the Radical Chemistry and Product Distribution in the OH-Initiated Oxidation of Benzene. *Environ. Sci. Technol.* **2020**, *54* (21), 13467-13477. DOI: https://doi.org/10.1021/acs.est.0c04780.

(7) Birdsall, A. W.; Elrod, M. J. Comprehensive NO-Dependent Study of the Products of the Oxidation of Atmospherically Relevant Aromatic Compounds. *J. Phys. Chem. A.* **2011**, *115* (21), 5397-5407. DOI: https://doi.org/10.1021/jp2010327.

(8) Nishino, N.; Arey, J.; Atkinson, R. Formation Yields of Glyoxal and Methylglyoxal from the Gas-Phase OH Radical-Initiated Reactions of Toluene, Xylenes, and Trimethylbenzenes as a Function of NO2 Concentration. *J. Phys. Chem. A.* **2010**, *114* (37), 10140-10147. DOI: https://doi.org/10.1021/jp105112h.

(9) Nehr, S.; Bohn, B.; Dorn, H. P.; Fuchs, H.; Haeseler, R.; Hofzumahaus, A.; Li, X.; Rohrer, F.; Tillmann, R.; Wahner, A. Atmospheric photochemistry of aromatic hydrocarbons: OH budgets during SAPHIR chamber experiments. *Atmos. Chem. Phys.* **2014**, *14* (13), 6941-6952. DOI: https://doi.org/10.5194/acp-14-6941-2014.

(10) Li, D.; Li, X.; Shao, M.; Liu, Y.; Lu, S. Comparative study on photochemical oxidation mechanism of toluene (in Chinese). *SCIENTIA SINICA Terrae* **2019**, *49* (04), 741-752. DOI: https://doi.org/10.1360/N072018-00077 From Cnki.

(11) He, S.; Liu, Y.; Song, M.; Li, X.; Lu, S.; Chen, T.; Mu, Y.; Lou, S.; Shi, X.; Qiu, X.; Zhu, T.; Zhang, Y. Insights into the Peroxide-Bicyclic Intermediate Pathway of Aromatic Photooxidation: Experimental Yields and NOx-Dependency of Ring-Opening and Ring-Retaining Products. *Environ. Sci. Technol.* **2023**, *57* (49), 20657-20668, Article. DOI: https://doi.org/10.1021/acs.est.3c05304 Scopus.

(12) He, S.; Liu, Y.; Song, M.; Li, X.; Lou, S.; Ye, C.; Liu, Y.; Liu, Y.; Ye, J.; Lu, S.; Zhou, W.; Qiu, X.; Zhu, T.; Zeng, L. Empirical Approach to Quantifying Sensitivity in Different Chemical Ionization Techniques for Organonitrates and Nitroaromatics Constrained by Ion–Molecule Reaction and Transmission Efficiency. *Anal. Chem.* **2024**, *96* (42), 16882-16890. DOI: https://doi.org/10.1021/acs.analchem.4c03751.

(13) Song, M.; He, S.; Li, X.; Liu, Y.; Lou, S.; Lu, S.; Zeng, L.; Zhang, Y. Optimizing the iodide-adduct chemical ionization mass spectrometry (CIMS) quantitative method for toluene oxidation intermediates: experimental insights into functional-group differences. *Atmos. Meas. Tech.* **2024**, *17* (17), 5113-5127. DOI: https://doi.org/10.5194/amt-17-5113-2024.

(14) Fuchs, H.; Hofzumahaus, A.; Rohrer, F.; Bohn, B.; Brauers, T.; Dorn, H. P.; Häseler, R.; Holland, F.; Kaminski, M.; Li, X.; Lu, K.; Nehr, S.; Tillmann, R.; Wegener, R.; Wahner, A. Experimental evidence for efficient hydroxyl radical regeneration in isoprene oxidation. *Nature Geoscience* **2013**, *6* (12), 1023-1026. DOI: https://doi.org/10.1038/ngeo1964.

(15) Rohrer, F.; Bohn, B.; Brauers, T.; Brüning, D.; Johnen, F. J.; Wahner, A.; Kleffmann, J. Characterisation of the photolytic HONO-source in the atmosphere simulation chamber SAPHIR. *Atmos. Chem. Phys.* **2005**, *5* (8), 2189-2201. DOI: https://doi.org/10.5194/acp-5-2189-2005.

(16) Bohn, B.; Zilken, H. Model-aided radiometric determination of photolysis frequencies in a sunlit atmosphere simulation chamber. *Atmos. Chem. Phys.* **2005**, *5* (1), 191-206. DOI: https://doi.org/10.5194/acp-5-191-2005.

(17) Lee, B. H.; Lopez-Hilfiker, F. D.; Mohr, C.; Kurten, T.; Worsnop, D. R.; Thornton, J. A. An Iodide-Adduct High-Resolution Time-of-Flight Chemical-Ionization Mass Spectrometer: Application to Atmospheric Inorganic and Organic Compounds. *Environ. Sci. Technol.* **2014**, *48* (11), 6309-6317. DOI: https://doi.org/10.1021/es500362a.

(18) Xu, L.; Coggon, M. M.; Stockwell, C. E.; Gilman, J. B.; Robinson, M. A.; Breitenlechner, M.; Lamplugh, A.; Crounse, J. D.; Wennberg, P. O.; Neuman, J. A.; Novak, G. A.; Veres, P. R.; Brown, S. S.; Warneke, C. Chemical ionization mass spectrometry utilizing ammonium ions (NH4+ CIMS) for measurements of organic compounds in the atmosphere. *Atmos. Meas. Tech.* **2022**, *15* (24), 7353-7373. DOI: https://doi.org/10.5194/amt-15-7353-2022.

(19) Yuan, B.; Koss, A. R.; Warneke, C.; Coggon, M.; Sekimoto, K.; de Gouw, J. A. Proton-Transfer-Reaction Mass Spectrometry: Applications in Atmospheric Sciences. *Chem. Rev.* **2017**, *117* (21), 13187-13229, Review. DOI: https://doi.org/10.1021/acs.chemrev.7b00325.

(20) Kaminski, M.; Fuchs, H.; Acir, I.-H.; Bohn, B.; Brauers, T.; Dorn, H.-P.; Häseler, R.; Hofzumahaus, A.; Li, X.; Lutz, A.; Nehr, S.; Rohrer, F.; Tillmann, R.; Vereecken, L.; Wegener, R.; Wahner, A. Investigation of the β-pinene photooxidation by OH in the atmosphere simulation chamber SAPHIR. *Atmos. Chem. Phys.* **2017**, *17* (11), 6631-6650. DOI: https://doi.org/10.5194/acp-17-6631-2017.

(21) Jenkin, M. E.; Saunders, S. M.; Pilling, M. J. The tropospheric degradation of volatile organic compounds: a protocol for mechanism development. *Atmos. Environ.* **1997**, *31* (1), 81-104. DOI: https://doi.org/10.1016/S1352-2310(96)00105-7.

(22) Kaminski, M.; Fuchs, H.; Acir, I. H.; Bohn, B.; Brauers, T.; Dorn, H. P.; Häseler, R.; Hofzumahaus, A.; Li, X.; Lutz, A.; Nehr, S.; Rohrer, F.; Tillmann, R.; Vereecken, L.; Wegener, R.; Wahner, A. Investigation of the β-pinene photooxidation by OH in the atmosphere simulation chamber SAPHIR. *Atmos. Chem. Phys.* **2017**, *17* (11), 6631-6650. DOI: https://doi.org/10.5194/acp-17-6631-2017.

(23) McMurry, P. H.; Grosjean, D. Gas and aerosol wall losses in teflon film smog chambers. *Environ. Sci. Technol.* **1985**, *19* (12), 1176-1182. DOI: https://doi.org/10.1021/es00142a006.

(24) Zhang, X.; Schwantes, R. H.; McVay, R. C.; Lignell, H.; Coggon, M. M.; Flagan, R. C.; Seinfeld, J. H. Vapor wall deposition in Teflon chambers. *Atmos. Chem. Phys.* **2015**, *15* (8), 4197-4214. DOI: https://doi.org/10.5194/acp-15-4197-2015.

(25) Crump, J. G.; Seinfeld, J. H. Turbulent deposition and gravitational sedimentation of an aerosol in a vessel of arbitrary shape. *J. Aerosol Sci* **1981**, *12* (5), 405-415, Article. DOI: https://doi.org/10.1016/0021-8502(81)90036-7.

(26) He, L.; Liu, W.; Li, Y.; Wang, J.; Kuwata, M.; Liu, Y. Wall loss of semi-volatile organic compounds in a Teflon bag chamber for the temperature range of 262–298 K: mechanistic insight

on temperature dependence. *Atmos. Meas. Tech.* **2024**, *17* (2), 755-764. DOI: 10.5194/amt-17-755-2024.

(27) Bates, K. H.; Jacob, D. J.; Li, K.; Ivatt, P. D.; Evans, M. J.; Yan, Y.; Lin, J. Development and evaluation of a new compact mechanism for aromatic oxidation in atmospheric models. *Atmos. Chem. Phys.* **2021**, *21* (24), 18351-18374. DOI: https://doi.org/10.5194/acp-21-18351-2021.

(28) Atkinson, R.; Aschmann, S. M.; Arey, J. Reactions of OH and NO3 radicals with phenol, cresols, and 2-nitrophenol at 296 ± 2 K. *Environ. Sci. Technol.* **1992**, *26* (7), 1397-1403. DOI: https://doi.org/10.1021/es00031a018.

(29) Sharma, S. B.; Mudaliar, M.; Rao, B. S. M.; Mohan, H.; Mittal, J. P. Radiation chemical oxidation of benzaldehyde, acetophenone, and benzophenone. *J. Phys. Chem. A.* **1997**, *101* (45), 8402-8408. DOI: https://doi.org/10.1021/jp9718717.

(30) Atkinson, R. Kinetics and mechanisms of the gas-phase reactions of the NO3 radical with organic-compounds. *J. Phys. Chem. Ref. Data* **1991**, *20* (3), 459-507. DOI: https://doi.org/10.1063/1.555887.

(31) Tyndall, G. S.; Staffelbach, T. A.; Orlando, J. J.; Calvert, J. G. Rate coefficients for the reactions of oh radicals with methylglyoxal and acetaldehyde. *Int. J. Chem. Kinet.* **1995**, *27* (10), 1009-1020. DOI: https://doi.org/10.1002/kin.550271006.

(32) Talukdar, R. K.; Zhu, L.; Feierabend, K. J.; Burkholder, J. B. Rate coefficients for the reaction of methylglyoxal (CH3COCHO) with OH and NO3 and glyoxal (HCO)2 with NO3. *Atmos. Chem. Phys.* **2011**, *11* (21), 10837-10851. DOI: https://doi.org/10.5194/acp-11-10837-2011.

(33) Martín, P.; Cabañas, B.; Colmenar, I.; Salgado, M. S.; Villanueva, F.; Tapia, A. Reactivity of E-butenedial with the major atmospheric oxidants. *Atmos. Environ.* **2013**, *70*, 351-360. DOI: https://doi.org/10.1016/j.atmosenv.2013.01.041.

(34) Liu, X. Y.; Jeffries, H. E.; Sexton, K. G. Atmospheric photochemical degradation of 1,4-unsaturated dicarbonyls. *Environ. Sci. Technol.* **1999**, *33* (23), 4212-4220. DOI: https://doi.org/10.1021/es990469y.

(35) Newland, M. J.; Rea, G. J.; Thüner, L. P.; Henderson, A. P.; Golding, B. T.; Rickard, A. R.; Barnes, I.; Wenger, J. Photochemistry of 2-butenedial and 4-oxo-2-pentenal under atmospheric boundary layer conditions. *Physical Chemistry Chemical Physics* **2019**, *21* (3), 1160-1171. DOI: https://doi.org/10.1039/c8cp06437g.

(36) Bierbach, A.; Barnes, I.; Becker, K. H.; Wiesen, E. Atmospheric chemistry of unsaturated carbonyls: butenedial, 4-oxo-2-pentenal, 3-hexene-2,5-dione, maleic-anhydride, 3H-furan-2-one, and 5-methyl-3H-furan-2-one. *Environ. Sci. Technol.* **1994**, *28* (4), 715-729. DOI: https://doi.org/10.1021/es00053a028.

(37) Roger, A.; Janet, A. Atmospheric degradation of volatile organic compounds. *Chem. Rev.* **2003**, *103* (12), 4605. DOI: https://doi.org/10.1021/cr0206420.

(38) Vereecken, L. Reaction Mechanisms for the Atmospheric Oxidation of Monocyclic Aromatic Compounds. In *Advances in Atmospheric Chemistry*, Advances in Atmospheric Chemistry, Vol. Volume 2; WORLD SCIENTIFIC, 2018; pp 377-527.

(39) Huang, M.; Wang, Z.; Hao, L.; Zhang, W. Theoretical investigation on the mechanism and kinetics of OH radical with m-xylene. *Comput. Theor. Chem.* **2011**, *965* (2-3), 285-290. DOI: https://doi.org/10.1016/j.comptc.2010.10.008.

(40) Wang, S.; Wu, R.; Berndt, T.; Ehn, M.; Wang, L. Formation of Highly Oxidized Radicals and Multifunctional Products from the Atmospheric Oxidation of Alkylbenzenes. *Environ. Sci. Technol.* **2017**, *51* (15), 8442-8449. DOI: https://doi.org/10.1021/acs.est.7b02374.

(41) Bandow, H.; Washida, N. Ring-cleavage reactions of aromatic hydrocarbons studied by FT-IR spectroscopy. II. Photooxidation of o-, m-, and p-xylenes in the NOx-air system. *Bulletin of The Chemical Society of Japan* **1985**, *58*, 2541-2548. DOI: https://doi.org/10.1246/bcsj.58.2541.

(42) Dumdei, B. E.; Kenny, D. V.; Shepson, P. B.; Kleindienst, T. E.; Nero, C. M.; Cupitt, L. T.; Claxton, L. D. MS/MS analysis of the products of toluene photooxidation and measurement of their mutagenic activity. *Environ. Sci. Technol.* **1988**, *22* (12), 1493-1498. DOI: https://doi.org/10.1021/es00177a017.

(43) Seuwen, R.; Warneck, P. Oxidation of toluene in NO chi free air: Product distribution and mechanism. *Int. J. Chem. Kinet.* **1996**, *28* (5), 315-332. DOI: https://doi.org/10.1002/(sici)1097-4601(1996)28:5<315::aid-kin1>3.0.co;2-y.

(44) Klotz, B.; Sorensen, S.; Barnes, I.; Becker, K. H.; Etzkorn, T.; Volkamer, R.; Platt, U.; Wirtz, K.; Martin-Reviejo, M. Atmospheric oxidation of toluene in a large-volume outdoor photoreactor: In situ determination of ring-retaining product yields. *J. Phys. Chem. A.* **1998**, *102* (50), 10289-10299. DOI: https://doi.org/10.1021/jp982719n.

(45) Smith, D. F.; McIver, C. D.; Kleindienst, T. E. Primary product distribution from the reaction of hydroxyl radicals with toluene at ppb NOX mixing ratios. *J. Atmos. Chem.* **1998**, *30* (2), 209-228. DOI: https://doi.org/10.1023/a:1005980301720.

(46) Zaytsev, A.; Koss, A. R.; Breitenlechner, M.; Krechmer, J. E.; Nihill, K. J.; Lim, C. Y.; Rowe, J. C.; Cox, J. L.; Moss, J.; Roscioli, J. R.; Canagaratna, M. R.; Worsnop, D. R.; Kroll, J. H.; Keutsch, F. N. Mechanistic study of the formation of ring-retaining and ring-opening products from the oxidation of aromatic compounds under urban atmospheric conditions. *Atmos. Chem. Phys.* **2019**, *19* (23), 15117-15129. DOI: https://doi.org/10.5194/acp-19-15117-2019.

(47) Atkinson, R.; Aschmann, S. M.; Arey, J. Formation of ring-retaining products from the OH radical-initated reactions of o-, m-, and p-xylene. *Int. J. Chem. Kinet.* **1991**, *23* (1), 77-97. DOI: https://doi.org/10.1002/kin.550230108.

(48) Smith, D. F.; Kleindienst, T. E.; McIver, C. D. Primary Product Distributions from the Reaction of OH with m-, p-Xylene, 1,2,4- and 1,3,5-Trimethylbenzene. *J. Atmos. Chem.* **1999**, *34* (3), 339-364. DOI: https://doi.org/10.1023/A:1006277328628.

(49) Zhao, J.; Zhang, R.; Misawa, K.; Shibuya, K. Experimental product study of the OH-initiated oxidation of m-xylene. *J. Photochem. Photobiol., A* **2005**, *176* (1-3), 199-207. DOI: https://doi.org/10.1016/j.jphotochem.2005.07.013.

(50) Baltaretu, C. O.; Lichtman, E. I.; Hadler, A. B.; Elrod, M. J. Primary Atmospheric Oxidation Mechanism for Toluene. *J. Phys. Chem. A.* **2009**, *113* (1), 221-230. DOI: https://doi.org/10.1021/jp806841t.

(51) Tuazon, E. C.; Macleod, H.; Atkinson, R.; Carter, W. P. L. Alpha-dicarbonyl yields from the NOx-air photooxidations of a series of aromatic-hydrocarbons in air. *Environ. Sci. Technol.* **1986**, *20* (4), 383-387. DOI: https://doi.org/10.1021/es00146a010.

(52) Tuazon, E. C.; Atkinson, R.; Macleod, H.; Biermann, H. W.; Winer, A. M.; Carter, W. P. L.; Pitts, J. N. Yields of Glyoxal and Methylglyoxal from The NOx-Air Photooxidations of Toluene and m-Xylene and p-Xylene. *Environ. Sci. Technol.* **1984**, *18* (12), 981-984. DOI: https://doi.org/10.1021/es00130a017.

(53) Pan, S.; Wang, L. Atmospheric oxidation mechanism of m-xylene initiated by OH radical. *Acta Physico-Chimica Sinica* **2015**, *31* (12), 2259–2268. DOI: https://doi.org/10.1021/jp506815v.

(54) Wang, L.; Wu, R.; Xu, C. Atmospheric oxidation mechanism of benzene. Fates of alkoxy radical intermediates and revised mechanism. *J. Phys. Chem. A.* **2013**, *117* (51), 14163. DOI: https://doi.org/10.1021/jp4101762.

(55) Shepson, P. B. E., E. O.; Corse, E. W. . Ring Fragmentation Reactions on the Photooxidations of Toluene and o-Xylene. . *J. Phys. Chem.* **1984**, *88*, 4122-4126.

(56) Gery, M. W.; Fox, D. L.; Jeffries, H. E.; Stockburger, L.; Weathers, W. S. A continuous stirred tank reactor investigation of the gas-phase reaction of hydroxyl radicals and toluene. *Int. J. Chem. Kinet.* **1985**, *17* (9), 931-955. DOI: https://doi.org/10.1002/kin.550170903.

(57) Volkamer, R.; Platt, U.; Wirtz, K. Primary and secondary glyoxal formation from aromatics: Experimental evidence for the bicycloalkyl-radical pathway from benzene, toluene, and p-xylene. *J. Phys. Chem. A.* **2001**, *105* (33), 7865-7874. DOI: https://doi.org/10.1021/jp010152w.

(58) Gomez Alvarez, E.; Viidanoja, J.; Munoz, A.; Wirtz, K.; Hjorth, J. Experimental confirmation of the dicarbonyl route in the photo-oxidation of toluene and benzene. *Environ. Sci. Technol.* **2007**, *41* (24), 8362-8369. DOI: https://doi.org/10.1021/es0713274.

(59) Jenkin, M. E.; Valorso, R.; Aumont, B.; Rickard, A. R.; Wallington, T. J. Estimation of rate coefficients and branching ratios for gas-phase reactions of OH with aromatic organic compounds for use in automated mechanism construction. *Atmos. Chem. Phys.* **2018**, *18* (13), 9329-9349. DOI: https://doi.org/10.5194/acp-18-9329-2018.

(60) Wang, S. N.; Newland, M. J.; Deng, W.; Rickard, A. R.; Hamilton, J. F.; Munoz, A.; Rodenas, M.; Vazquez, M. M.; Wang, L. M.; Wang, X. M. Aromatic Photo-oxidation, A New Source of Atmospheric Acidity. *Environ. Sci. Technol.* **2020**, *54* (13), 7798-7806. DOI: https://doi.org/10.1021/acs.est.0c00526.

(61) Bianchi, F.; Kurten, T.; Riva, M.; Mohr, C.; Rissanen, M. P.; Roldin, P.; Berndt, T.; Crounse, J. D.; Wennberg, P. O.; Mentel, T. F.; Wildt, J.; Junninen, H.; Jokinen, T.; Kulmala, M.; Worsnop, D. R.; Thornton, J. A.; Donahue, N.; Kjaergaard, H. G.; Ehn, M. Highly Oxygenated Organic Molecules (HOM) from Gas-Phase Autoxidation Involving Peroxy Radicals: A Key Contributor to Atmospheric Aerosol. *Chem. Rev.* **2019**, *119* (6), 3472-3509. DOI: https://doi.org/10.1021/acs.chemrev.8b00395.

(62) Molteni, U.; Bianchi, F.; Klein, F.; El Haddad, I.; Frege, C.; Rossi, M. J.; Dommen, J.; Baltensperger, U. Formation of highly oxygenated organic molecules from aromatic compounds. *Atmos. Chem. Phys.* **2018**, *18* (3), 1909-1921. DOI: https://doi.org/10.5194/acp-18-1909-2018.

(63) Stirnweis, L.; Marcolli, C.; Dommen, J.; Barmet, P.; Frege, C.; Platt, S. M.; Bruns, E. A.; Krapf, M.; Slowik, J. G.; Wolf, R.; Prevot, A. S. H.; Baltensperger, U.; El-Haddad, I. Assessing the influence of NOx concentrations and relative humidity on secondary organic aerosol yields from alpha-pinene photo-oxidation through smog chamber experiments and modelling calculations. *Atmos. Chem. Phys.* **2017**, *17* (8), 5035-5061. DOI: https://doi.org/10.5194/acp-17-5035-2017.

(64) Surratt, J. D.; Chan, A. W. H.; Eddingsaas, N. C.; Chan, M.; Loza, C. L.; Kwan, A. J.; Hersey, S. P.; Flagan, R. C.; Wennberg, P. O.; Seinfeld, J. H. Reactive intermediates revealed in secondary organic aerosol formation from isoprene. *Proc. Natl. Acad. Sci. USA.* **2010**, *107* (15), 6640-6645. DOI: https://doi.org/10.1073/pnas.0911114107.

(65) Qi, X.; Zhu, S.; Zhu, C.; Hu, J.; Lou, S.; Xu, L.; Dong, J.; Cheng, P. Smog chamber study of the effects of NOx and NH3 on the formation of secondary organic aerosols and optical properties from photo-oxidation of toluene. *Sci. Total Environ.* **2020**, *727*, 138632. DOI: https://doi.org/10.1016/j.scitotenv.2020.138632.

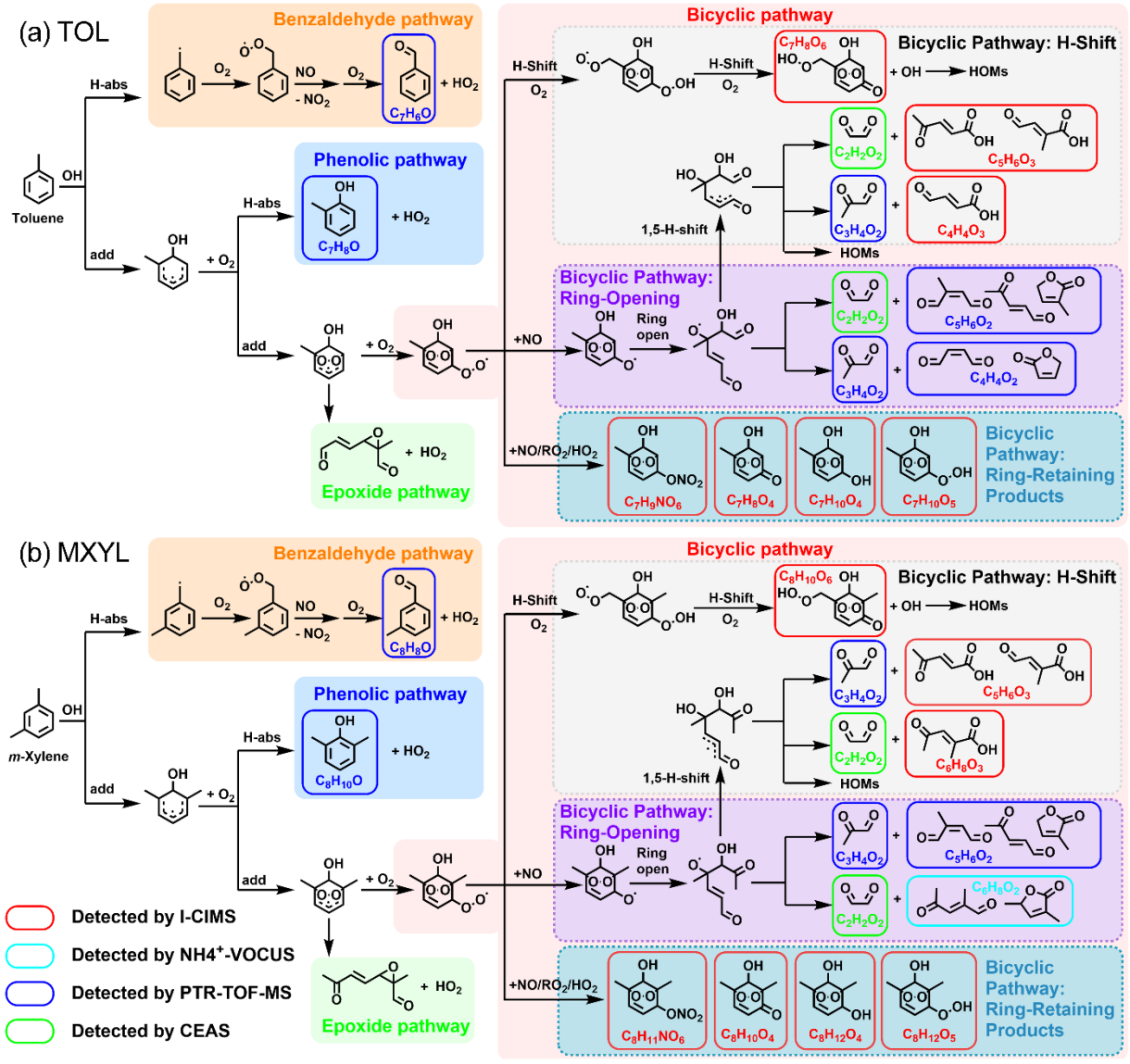

Scheme 1. (a-b) Schematic diagram of the oxidation process of aromatics. The key intermediate species that can be measured by I-CIMS are highlighted in red, those measurable by NH_4^+-VOCUS are highlighted in cyan, those measurable by PTR-TOF-MS are highlighted in blue, and those measurable by ICAD are highlighted in green.

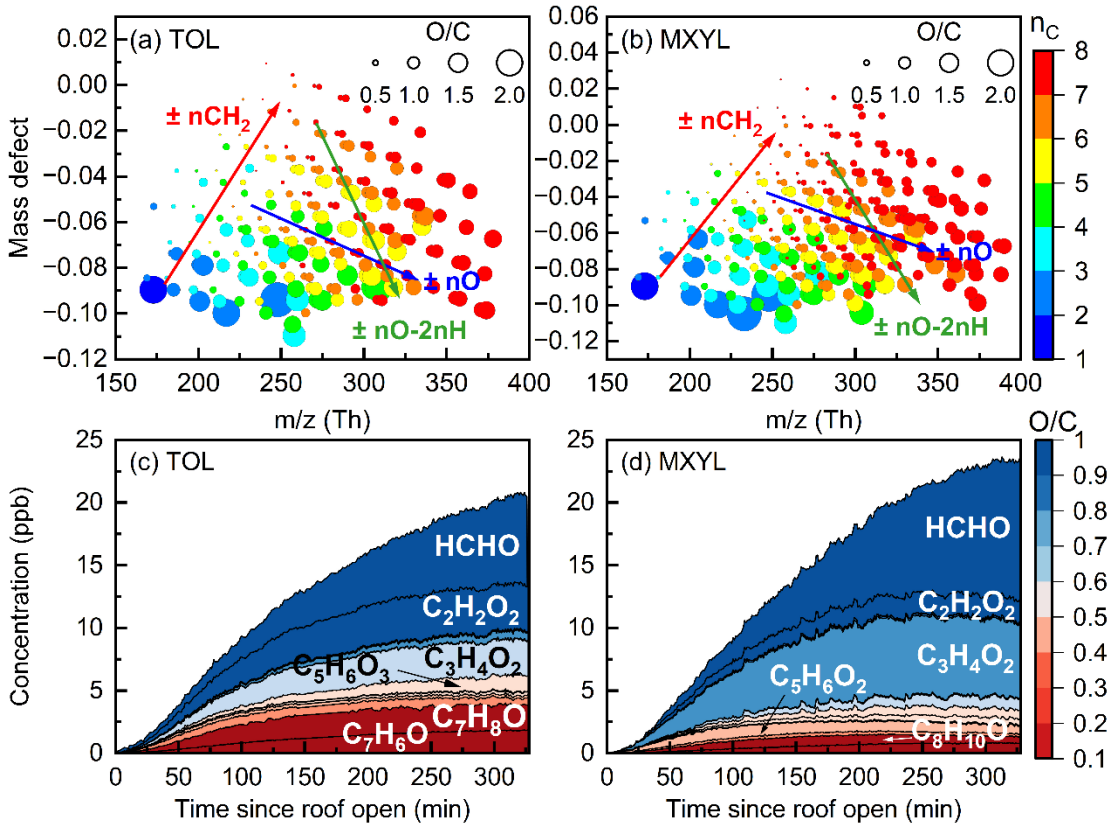

755

756 **Figure 1.** (a-b) High-resolution mass defect spectra of gas-phase products resulting from the
757 oxidation of toluene and m-xylene, measured via I-CIMS. (c-d) Time series of measured primary
758 oxidation products derived from toluene and m-xylene, with an initial NO concentration of
759 approximately 150 pptv.

760

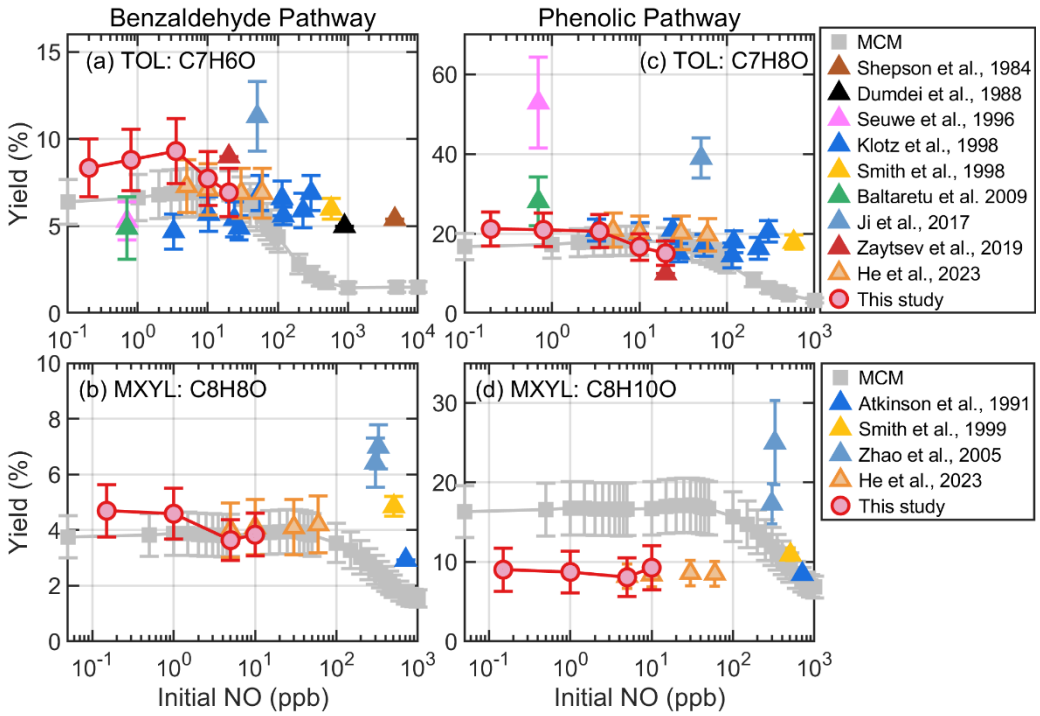

Figure 2. Yields of typical benzaldehyde pathway products: (a) benzaldehyde, and (b) methylbenzaldehyde under varying initial NO concentrations in toluene oxidation; Yield of typical phenolic pathway products: (c) cresol, and (d) dimethylphenol under varying initial NO concentrations in m-xylene oxidation.

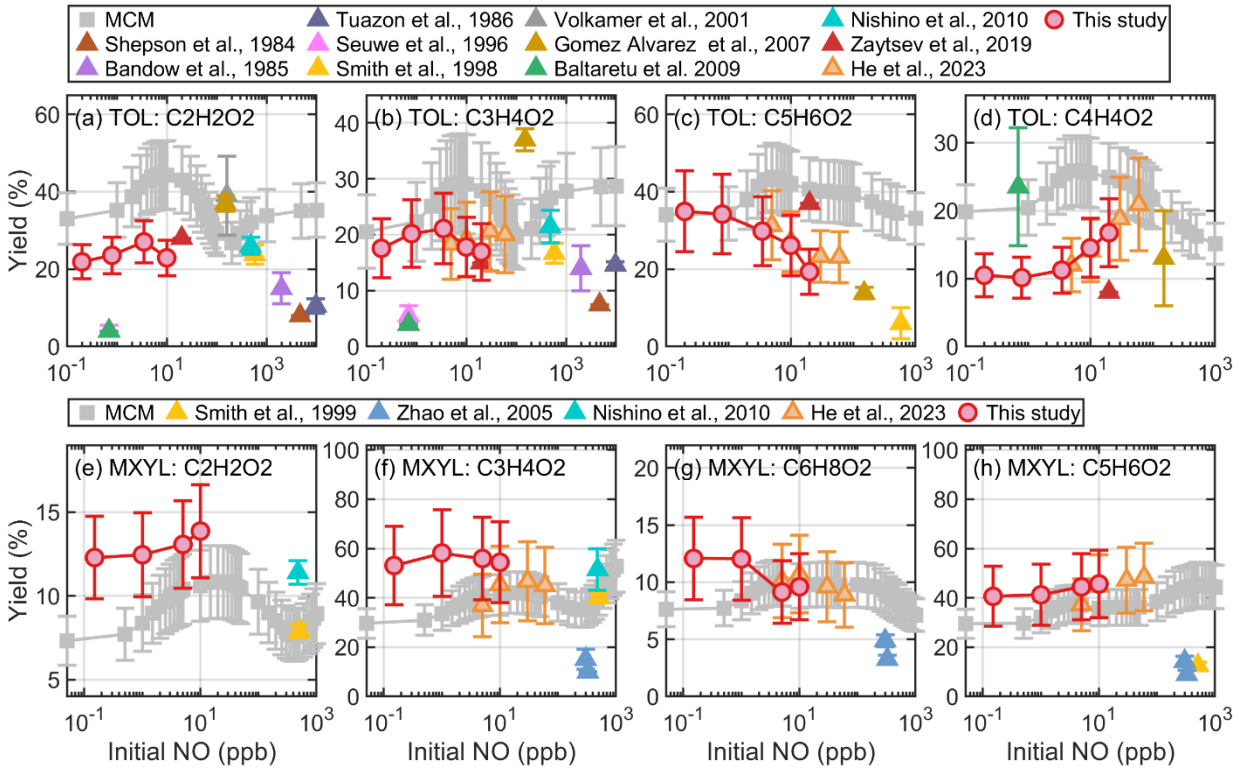

Figure 3. Yields of typical bicyclic pathway ring-opening products: (a) Glyoxal, (b) Methylglyoxal, (c) $C_5H_6O_2$, and (d) $C_4H_4O_2$ under varying initial NO concentrations in toluene oxidation; Yields of typical bicyclic pathway ring-opening products: (e) Glyoxal, (f) Methylglyoxal, (g) $C_6H_8O_2$, and (h) $C_5H_6O_2$ under varying initial NO concentrations in m-xylene oxidation.

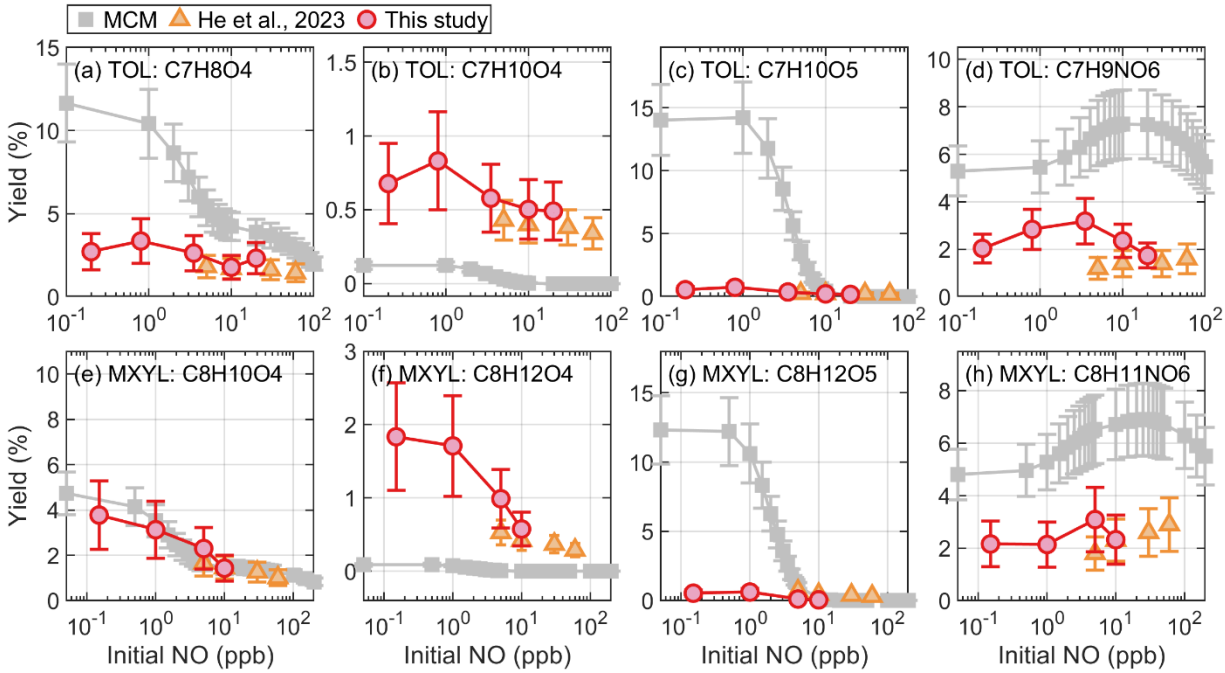

772

773 **Figure 4.** Yield distributions of typical bicyclic pathway ring-retaining products: (a) $C_7H_8O_4$, (b)
774 $C_7H_{10}O_4$, (c) $C_7H_{10}O_5$, and (d) $C_7H_9NO_6$ under Varying initial NO concentrations in toluene
775 oxidation; Yield distributions of typical bicyclic pathway ring-retaining products: (e) $C_8H_{10}O_4$, (f)
776 $C_8H_{12}O_4$, (g) $C_8H_{12}O_5$, and (h) $C_8H_{11}NO_6$ under Varying initial NO concentrations in m-xylene
777 oxidation.

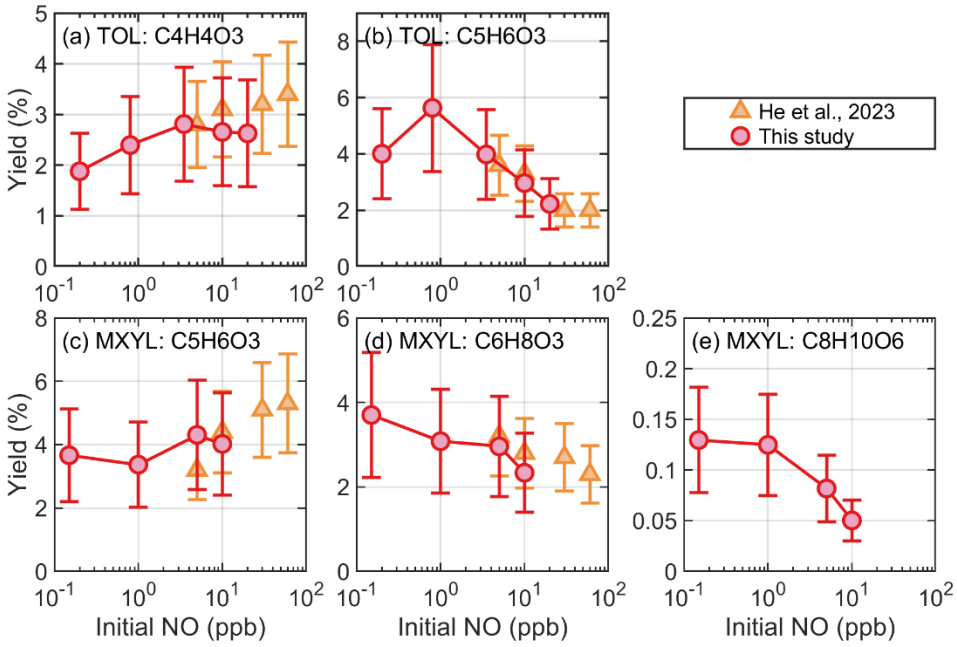

778

779 **Figure 5.** Yield distributions of H-shift new products: (a) $C_4H_4O_3$ and (b) $C_5H_6O_3$ under Varying
780 initial NO concentrations in toluene oxidation; Yield distributions of H-shift new products: (c)
781 $C_5H_6O_3$, (d) $C_6H_8O_3$, and (e) $C_8H_{10}O_6$ under Varying initial NO concentrations in m-xylene
782 oxidation.

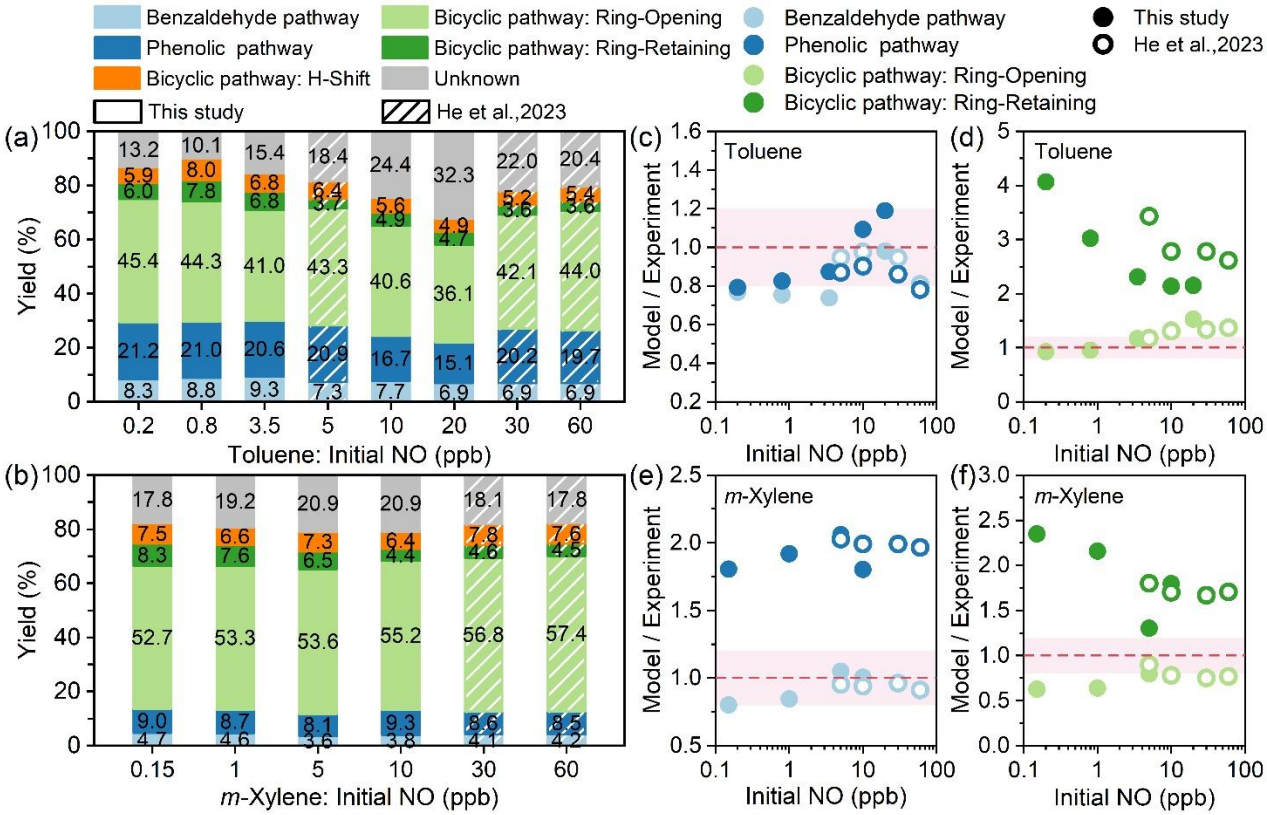

Figure 6. (a)-(b) Impact of initial NO concentrations on branching ratios of benzaldehyde, phenolic, and bicyclic pathways during toluene and m-xylene oxidation. (c)-(f) Variation of model-to-experimental yield ratios for benzaldehyde, phenolic, and bicyclic pathways during toluene and m-xylene oxidation at different initial NO concentrations.